Cite this: *J. Mater. Chem. A*, 2019, 7, 19970

# A borate decorated anion-immobilized solid polymer electrolyte for dendrite-free, long-life Li metal batteries†

Cheng Ma,<sup>a</sup> Yiming Feng,<sup>a</sup> Fangzhou Xing,<sup>a</sup> Lin Zhou,<sup>a</sup> Ying Yang,<sup>a</sup> Qingbing Xia,<sup>b</sup> Liangjun Zhou,<sup>a</sup> Lijun Zhang,<sup>a</sup> Libao Chen,<sup>b</sup> Douglas G. Ivey,<sup>c</sup> Donald R. Sadoway<sup>d</sup> and Weifeng Wei<sup>\*a</sup>

Abrupt Li dendrite growth and the safety hazards caused by liquid electrolytes are generally acknowledged as major technical barriers for the practical application of Li metal batteries. Solid polymer electrolytes (SPEs) are promising to overcome these obstacles, but suffer from rigidity–conductivity inconsistency, ununiform ion distribution and inferior interfacial compatibility. Herein, an anion-immobilized SPE using vinylene carbonate as the rigid polymer backbone and flexible ether oxygen chains containing anion-trapping boron moieties is proposed, which facilitates the Li<sup>+</sup> transport and adjusts the ion distribution. This ingenious design along with facile *in situ* preparation effectively integrates a favorable Young's modulus (2.41 GPa), high ionic conductivity ( $9.11 \times 10^{-4}$  S cm<sup>-1</sup> at 25 °C) and a high Li<sup>+</sup> transference number (0.68), as well as achieving a stable solid electrolyte interface layer. As a result, these integrative properties enable dendrite-free LiFePO<sub>4</sub>/Li batteries with excellent rate capacity (8C, 98.3 mA h g<sup>-1</sup>) and superior long-term cyclability over 600 cycles at 30 °C, providing a new strategy for safe and high-energy all-solid-state energy storage systems.

Received 12th July 2019  
Accepted 2nd August 2019

DOI: 10.1039/c9ta07551h

rsc.li/materials-a

## Introduction

Rechargeable batteries with the virtues of high safety, high-energy density and low cost are urgently needed to meet the expanding demand for future energy storage systems.<sup>1,2</sup> Li metal batteries (LMBs) have attracted much attention as next generation advanced battery technology due to the high theoretical specific capacity (3860 mA h g<sup>-1</sup>), low density (0.534 g cm<sup>-3</sup>) and the lowest reduction potential (−3.040 V vs. the standard hydrogen electrode (SHE)) of Li metal.<sup>3–5</sup> However, potential issues such as short lifetime and short-circuiting, which result from the continuous growth of Li dendrites during repetitive Li plating and stripping, impede the significant development of LMBs.<sup>5–7</sup> Some advances in preventing Li dendrite growth have been achieved *via* optimizing the chemical components of electrolytes,<sup>8,9</sup> engineering functional separators,<sup>10,11</sup> artificial fabrication of solid electrolyte interface (SEI) layers,<sup>12,13</sup> constructing three-

dimensional (3D) current collectors,<sup>14,15</sup> *etc.* However, most efforts are limited by intrinsic safety concerns, ranging from uncontrolled side reactions at the Li anode interface to underlying risks (leakage, fires and explosions) related to liquid electrolytes (LEs).<sup>16</sup>

Solid state electrolytes, especially solid polymer electrolytes (SPEs), present a promising route to enhancing the safety performance and may enable dendrite-free all-solid-state LMBs owing to their high thermal and electrochemical stability, as well as the reduced side reactions with the Li metal anode.<sup>17,18</sup> Despite the progress achieved in mechanically blocking dendrite growth by SPEs with moderate mechanical strength,<sup>19,20</sup> it's difficult to avoid the penetration of dendritic Li merely by improving the shear modulus, owing to the inevitable uneven electrodeposition behavior of Li. Chazalviel *et al.* revealed that the anion depletion near the Li electrode leads to a space-charge region that accounts for ramified depositions,<sup>5,21</sup> while anion-immobilized electrolytes with high ionic conductivity can facilitate the regulation of the ion distribution to achieve uniform Li deposits.<sup>22,23</sup> Besides, the interfacial chemistry stability relevant to the SEI also has a great effect on initial dendrite seeds and inhomogeneous nucleation.<sup>3,24,25</sup> Nevertheless, it still remains a great challenge to effectively design SPEs with all these excellent characteristics of reliable mechanical strength, high ion mobility to regulate Li depositing behavior, and being feasible to form a stable interface with the lithium anode.

From this perspective, we have designed an anion-immobilized solid state polymer electrolyte (denoted as P(V-B)) *via*

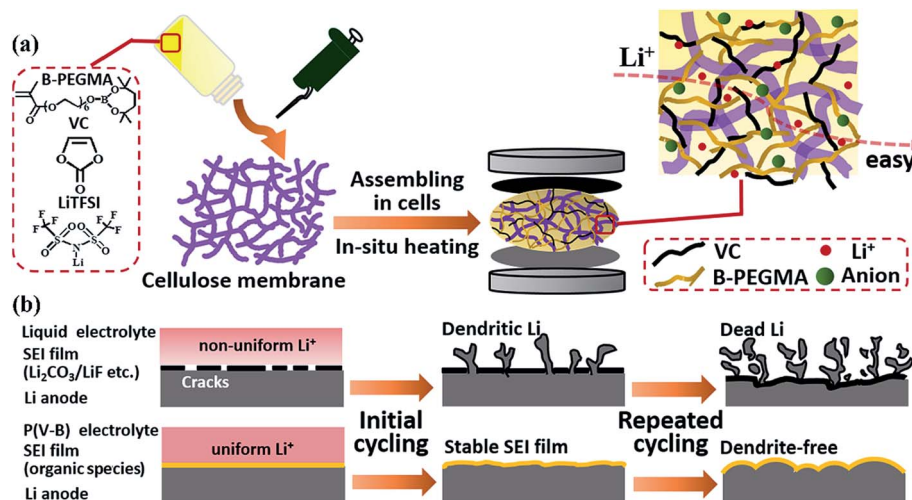
<sup>a</sup>State Key Laboratory of Powder Metallurgy, Central South University, Changsha, Hunan 410083, People's Republic of China. E-mail: weifengwei@csu.edu.cn

<sup>b</sup>Institute for Superconducting and Electronic Materials, University of Wollongong, Wollongong, New South Wales, 2522, Australia

<sup>c</sup>Department of Chemical & Materials Engineering, University of Alberta, Edmonton, Alberta, Canada T6G 1H9

<sup>d</sup>Department of Materials Science and Engineering, Massachusetts Institute of Technology, Cambridge, Massachusetts 02139-4307, USA

† Electronic supplementary information (ESI) available. See DOI: 10.1039/c9ta07551h



Scheme 1 (a) Illustration of the fabrication of the P(V-B) electrolyte *via in situ* polymerization. (b) Schematic of Li anode structure evolution with a LE and the P(V-B) electrolyte during cycling.

a facile *in situ*, one step polymerization of rigid vinylene carbonate (VC) and flexible poly(ethylene glycol) methyl ether methacrylate containing cyclic boroxane groups (B-PEGMA) on a cellulose membrane framework, as illustrated in Scheme 1a. The as-prepared flexible P(V-B) electrolyte presents desirable physical, mechanical and electrochemical properties, including: (i) good mechanical stability with an average Young's modulus of 2.41 GPa; (ii) high ionic conductivity of  $9.11 \times 10^{-4}$  S cm<sup>-1</sup> at 25 °C, resulting from the enhanced interaction with Li salts and segmental mobility by the ether oxygen (EO) moieties; and (iii) high Li<sup>+</sup> transference number of 0.68 and exceptional interfacial stability against random Li<sup>+</sup> plating/stripping

behavior, which is contributed by the boron moieties immobilizing anions, leading to a dendrite-free Li anode (Scheme 1b). With all these advantages, a solid-state Li metal battery based on the P(V-B) electrolyte has demonstrated excellent long-term cycling stability, superior rate performance, attractive mechanical stability and good flexibility.

## Results and discussion

The P(V-B) SPE was synthesized *via in situ* polymerization of a solution precursor obtained by mixing LiTFSI, VC and B-PEGMA organic monomers. A cellulose membrane (CM),

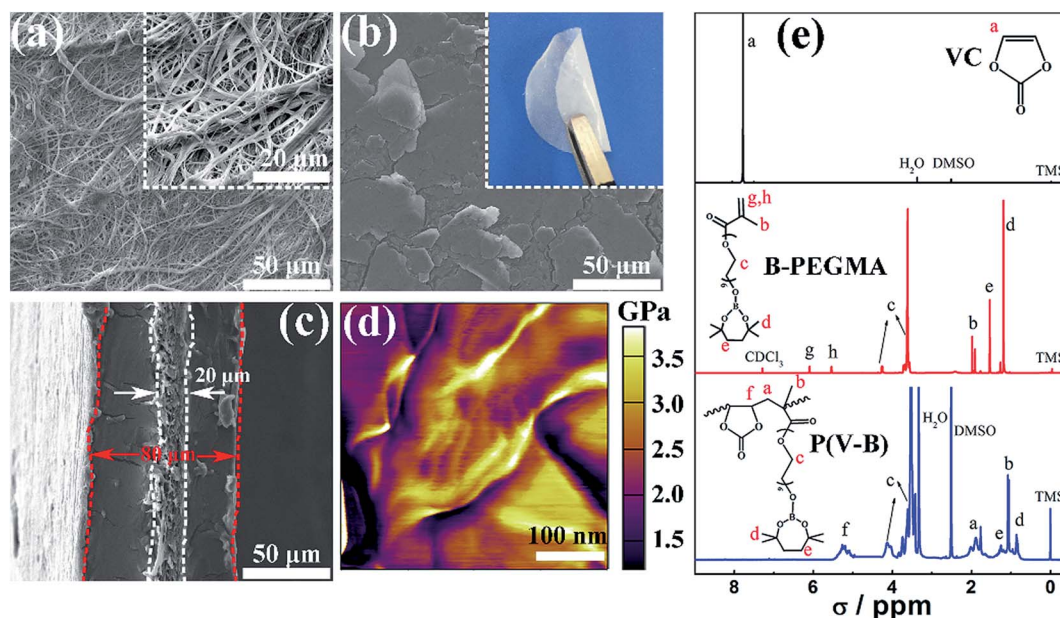


Fig. 1 (a) SEM image of the surface morphology of the bare CM. (b) Top-view SEM image of the P(V-B) electrolyte with an optical photograph (inset) and (c) cross-sectional SEM image of the P(V-B) electrolyte. (d) Young's modulus mapping of the P(V-B) electrolyte and (e) <sup>1</sup>H NMR spectra of VC, B-PEGMA and as-synthesized P(V-B).

consisting of copious irregularly shaped holes formed by randomly arranged nanofibers (Fig. 1a), was selected as the mechanical framework. Meanwhile, the high porosity and enriched oxygen functional groups (Fig. S1, ESI<sup>†</sup>) endow the CM with excellent affinity for organic solvents.<sup>26</sup> After polymerization, the solution precursor is transformed into a solid polymer electrolyte (Fig. S2<sup>†</sup>), and the obtained P(V-B) electrolyte exhibits appreciable flexibility (Fig. 1b). The cross-sectional scanning electron microscopy (SEM) image (Fig. 1c) shows that the electrolyte components uniformly cover both sides of the CM framework and infiltrate evenly into the internal pores. The <sup>1</sup>H nuclear magnetic resonance (NMR) spectra in Fig. 1e show a new signal (marked as f) that appears at 5.2 ppm in addition to the disappearance of the signals of the vinyl groups (marked as a and g, h) from VC and B-PEGMA, demonstrating the formation of the final P(V-B) copolymer, which was further verified by Fourier transform infrared spectroscopy (Fig. S3<sup>†</sup>). The differential scanning calorimetry (DSC) analysis (Fig. S4a<sup>†</sup>) shows no melting peak in the temperature range from -60 to 60 °C, which reveals the amorphous nature of the P(V-B) electrolyte along with the XRD pattern (Fig. S4b<sup>†</sup>). Specifically, the glass transition temperature (*T*<sub>g</sub>) of ~22.5 °C for the poly(vinyl chloride) (P(V)) electrolyte decreases to ~2.3 °C in the P(V-B) electrolyte, indicating its superior chain mobility and lower activation

energy (*E*<sub>a</sub>) for Li<sup>+</sup> transport.<sup>27</sup> The P(V-B) electrolyte also exhibits desirable mechanical properties with an average Young's modulus of 2.41 GPa (Fig. 1d) and a maximum tensile stress of 9.6 MPa (2.3 MPa for the CM, Fig. S5<sup>†</sup>), which can effectively alleviate Li dendrite penetration.<sup>28</sup> Thermal degradation of the P(V-B) electrolyte occurs at ~277 °C, confirming its superior thermal and dimensional stability (Fig. S6<sup>†</sup>).

The Arrhenius plots in Fig. 2a and S7<sup>†</sup> reveal that the P(V-B) electrolyte possesses the highest ionic conductivity of  $9.11 \times 10^{-4} \text{ S cm}^{-1}$  with a VC/B-PEGMA ratio of 4/1, which is about 50 times that of the P(V) electrolyte ( $1.83 \times 10^{-5} \text{ S cm}^{-1}$ ), and is superior to the values reported in the literature (Table S1, ESI<sup>†</sup>).<sup>27,29–35</sup> Simulation results on the electron cloud density distribution of the molecular model show that the oxygen atoms in both the C=O and the C-O-C groups are negatively charged, which verifies that the improved ionic conductivity should be ascribed to the enhanced interactions between Li<sup>+</sup> and the highly mobile EO groups with lower natural bond orbital (NBO) charge (Fig. 3a). Moreover, the conductivity exhibits an Arrhenius-type behavior with temperature, and the decreased value of the activation energy (*E*<sub>a</sub>) (Table S2<sup>†</sup>) also demonstrates that the introduced flexible B-PEGMA segment is effective in reducing the energy barrier for Li<sup>+</sup> transmission.<sup>36</sup>

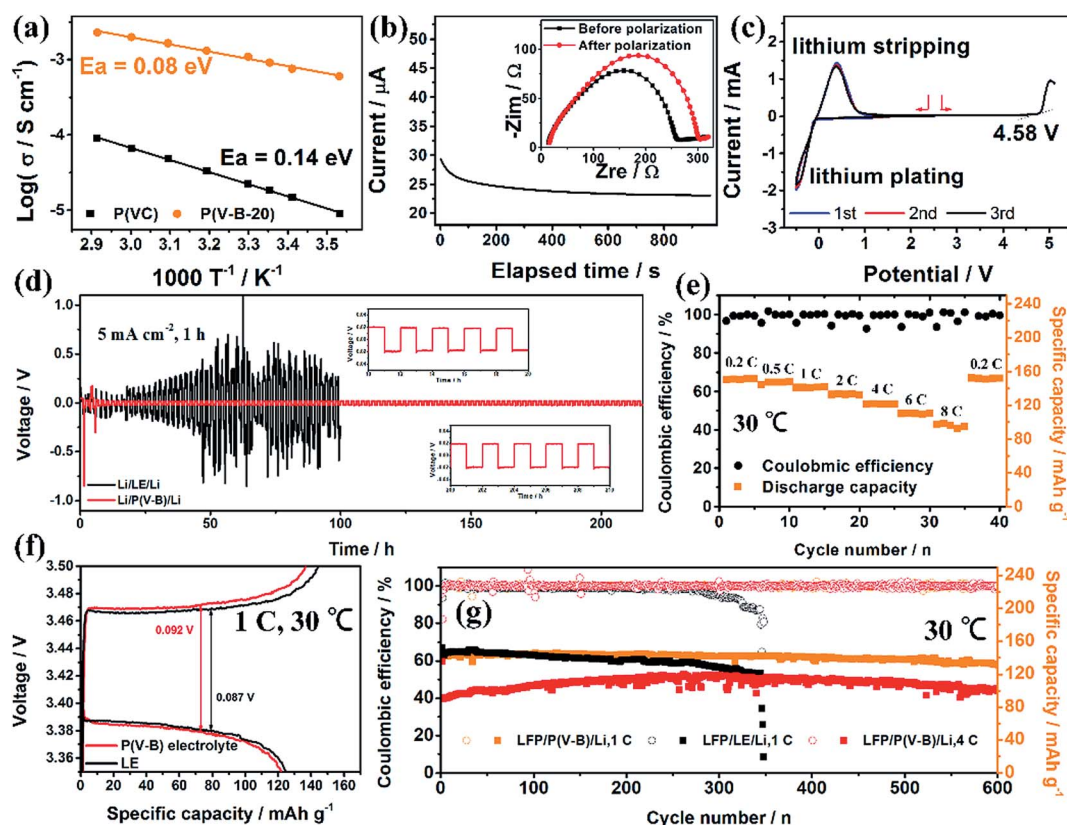


Fig. 2 (a) Arrhenius plots at temperatures from 10 to 70 °C for P(V) and the P(V-B) electrolyte. (b) Current–time plot of a symmetric Li/P(V-B) electrolyte/Li cell and AC impedance spectra (inset) before and after polarization. (c) Cyclic voltammograms for the first 3 cycles of the P(V-B) electrolyte. (d) Voltage profiles of Li plating/stripping in symmetric Li cells containing a LE (black) and the P(V-B) electrolyte (red) at a current density of  $5 \text{ mA cm}^{-2}$  for 1 h, with the insets showing enlargements of the indicated time periods. (e) Rate capability of the LFP/P(V-B) electrolyte/Li battery. (f and g) Comparison of the charge and discharge voltage gap (f) and cycling performance (g) of LFP/Li metal batteries with a LE and the P(V-B) electrolyte at 30 °C.

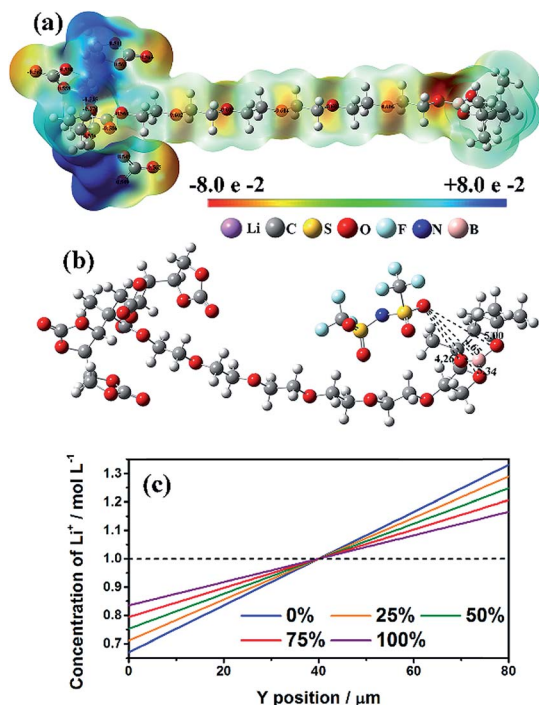


Fig. 3 (a and b) Geometrical structure of the model unit in P(V-B) with probable electron cloud density distribution (a) and binding energy of anions to the boronic ester groups (b). (c) Simulation of  $\text{Li}^+$  distribution from the Li anode surface to the bulk electrolyte in a steady state with various proportions of immobilized anions.

The  $\text{Li}^+$  transference number ( $t_{\text{Li}^+}$ ) of the P(V-B) electrolyte was calculated to be approximately 0.68, which is higher than the values of 0.43 and 0.26 for the P(VC) electrolyte and the LE, respectively (Fig. S8, Table S3†). Density functional theory (DFT) calculations, based on the Lee–Yang–Parr correlation energy functional, show that the interaction energy between the boronic ester group and the anion is  $-36.89 \text{ kJ mol}^{-1}$  with a short B–O distance of 4.65 Å (Fig. 3b). All of the above results demonstrate that boron with an empty p-orbital can immobilize anions by electronic interaction.<sup>37,38</sup> More importantly, anion immobilization is beneficial for decreasing the  $\text{Li}^+$  concentration gradient from the bulk electrolyte to the anode surface (Fig. 3c), which could reduce the electric field at the metal electrode and further lead to uniform Li deposition behavior.<sup>22,39</sup> Moreover, compared to the low oxidative decomposition potential ( $<4.5 \text{ V}$ ) of conventional  $\text{LiPF}_6$ -based carbonate electrolytes,<sup>40</sup> the P(V-B) electrolyte is electrochemically stable within 4.58 V vs.  $\text{Li}/\text{Li}^+$  and displays a pair of highly reversible lithium redox peaks (Fig. 2c).

The electrochemical behavior of dynamic  $\text{Li}^+$  plating/stripping was detected by galvanostatic polarization tests. Symmetric Li cells using the P(V-B) electrolyte have a smaller polarization potential and more stable long-term cycling without over-potential increments than LE based cells (Fig. 2d and S9a–c†). Its excellent performance reveals that the P(V-B) electrolyte could enable outstanding interfacial compatibility with Li metal and facilitate the formation of an

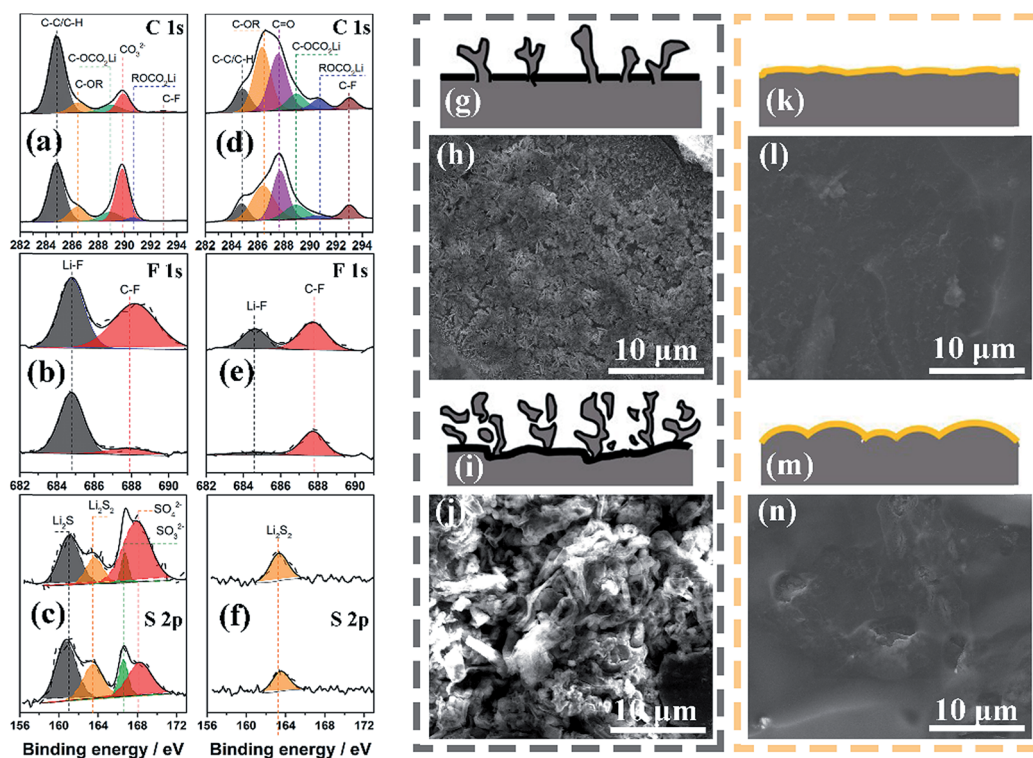


Fig. 4 (a–f) XPS spectra of C 1s (a and d), F 1s (b and e) and S 2p (c and f) for Li anodes from LFP/Li metal batteries with a LE (a–c) and the P(V-B) electrolyte (d–f) after 1 (top) and 50 cycles (bottom) at 1C. (g–n) SEM SE images and schematic cross sections of Li anodes from LFP/Li metal batteries with a LE (g–j) and the P(V-B) electrolyte (k–n) after 50 (g, h, k, and l) and 100 cycles (i, j, m, and n) respectively.

electrochemically sustainable SEI film, which is also confirmed by the relatively constant interface impedance over time (Fig. S10†).

LiFePO<sub>4</sub> (LFP)/Li metal batteries were fabricated to further evaluate the feasibility of the P(V-B) electrolyte. At 30 °C, owing to its high ionic conductivity and low interfacial resistance (Fig. S10a†), the discharge capacity of such a battery can remain at 98.3 mA h g<sup>-1</sup> at 8C (Fig. 2e and S11b†). Importantly, the polarization between the charge/discharge curves is 0.092 V at 1C (Fig. 2f), which is comparable to that with the LE, and the capacity retention for the LFP/P(V-B) electrolyte/Li battery is up to 93.3% after 600 cycles with respect to the initial capacity of 141.2 mA h g<sup>-1</sup>. Even at a high current density of 4C, the P(V-B) based LFP/Li battery still delivers a discharge capacity of 102.2 mA h g<sup>-1</sup> after 600 cycles. For the LE based battery, a short circuit appeared along with reduced coulombic efficiency upon cycling (Fig. 2g). It is remarkable that such exceptional battery performance can also be achieved in a large temperature range

from 10 °C to 60 °C (Fig. S12†), further suggesting the electrochemical stability and attractive interfacial kinetic behavior of the P(V-B) electrolyte. In addition, we also test the P(V-B) electrolyte in a LiNi<sub>0.6</sub>Co<sub>0.2</sub>Mn<sub>0.2</sub>O<sub>2</sub>/Li battery with a higher cut-off voltage, and the reversible capacity stabilizes at 115 mA h g<sup>-1</sup> after 100 cycles at 30 °C and 1C (Fig. S13†), highlighting its outstanding interface compatibility with high-voltage cathode materials.

The interfacial properties of the cycled Li anodes taken from LFP/Li metal batteries with a LE and the P(V-B) electrolyte was studied. High-resolution X-ray photoelectron spectra (XPS) show that a SEI film comprised of decomposed organics and massive inorganic species (Li<sub>2</sub>CO<sub>3</sub>, LiF and Li<sub>x</sub>S<sub>y</sub>/Li<sub>x</sub>SO<sub>y</sub>) were formed on the surface of the Li anode after the initial cycling in the LE based cells, and the chemical constituents change dramatically in the subsequent cycles, accompanied by the constant consumption of the Li metal and electrolyte (Fig. 4a-c). In contrast, the organic species with high ion transfer

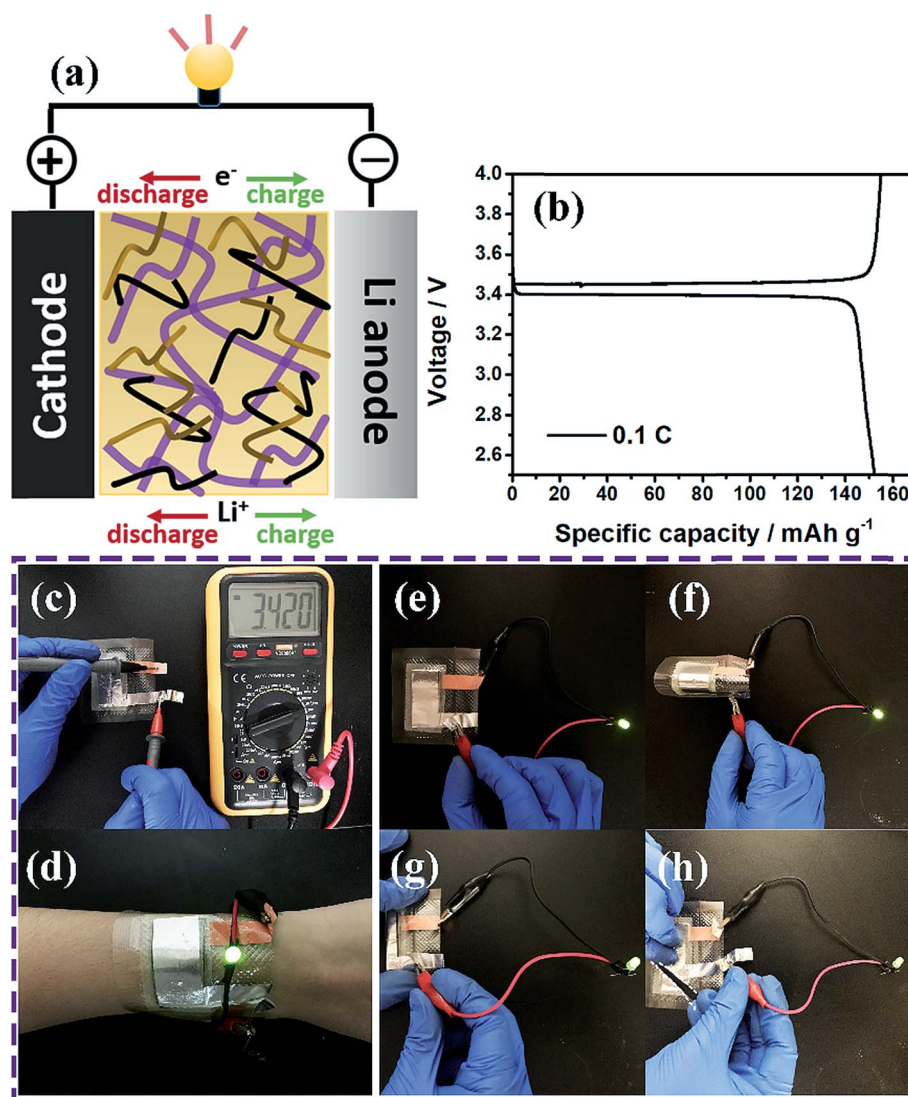


Fig. 5 Schematic illustration of a flexible LFP/Li metal pouch cell (a) and the corresponding galvanostatic discharge/charge profile (b) based on voltage testing (c), and photographs of the pouch cell lighting a LED lamp in flat and bent states (d–g), and even after having a corner cut off (h).

kinetics primarily constitute the pristine native SEI layer for the LFP/Li battery with the P(V-B) electrolyte. In particular, there are no obvious changes in the concentrations of the organic species, while the proportion of the inorganic phases (LiF and  $\text{Li}_x\text{S}_y$ ) decreases on the surface of the Li anode after 50 cycles (Fig. 4d–f). SEM images reveal that, with the LE electrolyte, dendritic Li cluster whiskers partially cover the anode surface initially (50 cycles, Fig. 4g, h, S14a and b†) and then completely cover the anode surface (100 cycles, Fig. 4i, j, S14 c and d†). The whiskers then break from their roots to become isolated Li whiskers (known as dead Li), culminating in a mossy, porous and highly resistant surface layer, which is well consistent with the performance degradation of the LFP/LE/Li battery. In contrast, the surface of the Li anode in the P(V-B) based battery is smooth and compact without cracks (Fig. 4k, l S14 e and f†), and forms no dendrites even after 100 cycles (Fig. 4m, n, S14 g and h†). All the above discrepancies demonstrate the synergy between adequate mechanical strength, decreased concentration polarization, and the stable interface enabled by the P(V-B) electrolyte, which can reduce side reactions and realize uniform  $\text{Li}^+$  electrodeposition. Moreover, such outstanding effects are also demonstrated by the electrochemical performance and interface information of Li/Cu asymmetric cells (see Fig. S15 in the ESI† for details).

To demonstrate the attractive flexible characteristics and potential applications of the P(V-B) electrolyte in wearable devices, a single layer soft-package cell with a flexible LFP cathode (Fig. S16†) and Li foil as the anode was fabricated and exhibits flat plateaus in both charge and discharge profiles (Fig. 5a and b). It is noteworthy that the cell can light a commercial green light-emitting diode lamp under different bending and folding orientations even after a corner has been cut (Fig. 5c–h), indicating that the P(V-B) electrolyte with good mechanical integrity and flexibility holds promise for wearable and other flexible devices.

## Conclusion

In summary, we have demonstrated an *in situ* strategy to construct a borate decorated anion-immobilized SPE for all solid state LMBs, which achieves adequate mechanical strength, superior ionic conductivity and an enhanced  $\text{Li}^+$  transference number. With the high-performance P(V-B) electrolyte, the assembled LMB exhibits long-term cycling stability without dendrite formation on the Li anode at various temperatures (10–60 °C). Simulation and characterization results indicate that the stable performance is attributable to the *in situ* formation of an electrochemically stable interface which eliminates inhomogeneous dendrite nucleation, anion-immobilization by borate groups to regulate non-uniform deposits and the adequate mechanical strength to suppress dendritic Li growth. This combination of innovative synthesis design and facile fabrication provides new insights into interfacial stabilization, Li dendrite inhibition and eventual practical applications of high-energy and safe LMBs.

## Author contributions

C. M. and W. F. W. conceived the idea and wrote the paper. C. M., L. Z. and Y. Y. synthesized the materials. C. M., Q. B. X., and L. J. Z. performed the material tests and characterization. Y. M. F. conducted the density functional theory calculations. F. Z. X. and L. J. Z. provided methods and software for the simulation of  $\text{Li}^+$  concentration distribution. M. C., Q. B. X., L. B. C. and W. F. W. performed the data analyses. D. G. I. and D. R. S. provided assistance with interpretation of the data and made revisions to the manuscript. All authors have given approval to the final version of the manuscript.

## Conflicts of interest

There are no conflicts to declare.

## Acknowledgements

The authors would like to acknowledge financial support from the National Key R&D Program of China (Grant No. 2018YFB0104200).

## Notes and references

- 1 J. M. Tarascon and M. Armand, *Nature*, 2001, **414**, 359–367.
- 2 B. Scrosati, J. Hassoun and Y. K. Sun, *Energy Environ. Sci.*, 2011, **4**, 3287–3295.
- 3 D. C. Lin, Y. Y. Liu and Y. Cui, *Nat. Nanotechnol.*, 2017, **12**, 194–206.
- 4 P. G. Bruce, S. A. Freunberger, L. J. Hardwick and J. M. Tarascon, *Nat. Mater.*, 2012, **11**, 19.
- 5 (a) J. N. Chazalviel, *Phys. Rev. A*, 1990, **42**, 7355; (b) C. Brissot, M. Rosso, J. N. Chazalviel and S. Lascaud, *J. Power Sources*, 1999, **81**, 925.
- 6 Y. M. Sun, N. Liu and Y. Cui, *Nat. Energy*, 2016, **1**, 16071.
- 7 X. B. Cheng, R. Zhang, C. Z. Zhao and Q. Zhang, *Chem. Rev.*, 2017, **117**, 10403–10473.
- 8 L. Suo, Y. S. Hu, H. Li, M. Armand and L. Q. Chen, *Nat. Commun.*, 2013, **4**, 1481.
- 9 Y. Lu, Z. Tu and L. A. Archer, *Nat. Mater.*, 2014, **13**, 961–969.
- 10 K. Liu, D. Zhuo, H. W. Lee, W. Liu, D. Lin, Y. Lu and Y. Cui, *Adv. Mater.*, 2017, **29**, 1603987.
- 11 Y. D. Liu, Q. Liu, L. Xin, Y. Z. Liu, F. Yang, E. A. Stach and J. Xie, *Nat. Energy*, 2017, **2**, 17083.
- 12 B. Zhu, Y. Jin, X. Z. Hu, Q. H. Zheng, S. Zhang, Q. J. Wang and J. Zhu, *Adv. Mater.*, 2017, **29**, 1603755.
- 13 R. Xu, X. Q. Zhang, X. B. Cheng, H. J. Peng, C. Z. Zhao, C. Yan and J. Q. Huang, *Adv. Funct. Mater.*, 2018, **28**, 1705838.
- 14 K. Yan, Z. D. Lu, H. W. Lee, F. Xiong, P. C. Hsu, Y. Z. Li, J. Zhao, S. Chu and Y. Cui, *Nat. Energy*, 2016, **1**, 16010.
- 15 P. Zou, Y. Wang, S. W. Chiang, X. Wang, F. Kang and C. Yang, *Nat. Commun.*, 2018, **9**, 464.
- 16 P. G. Balakrishnan, R. Ramesh and T. P. Kumar, *J. Power Sources*, 2006, **155**, 401–414.
- 17 J. B. Goodenough, *Energy Environ. Sci.*, 2014, **7**, 14–18.

- 18 K. K. Fu, Y. Gong, B. Liu, Y. Zhu, S. Xu, Y. Yao, W. Luo, C. Wang, S. D. Lacey, J. Dai, Y. Chen, Y. Mo, E. Wachsman and L. Hu, *Sci. Adv.*, 2017, **3**, e1601659.
- 19 C. P. Yang, K. Fu, Y. Zhang, E. Hitz and L. B. Hu, *Adv. Mater.*, 2017, **29**, 1701169.
- 20 Q. Pan, D. M. Smith, H. Qi, S. Wang and C. Y. Li, *Adv. Mater.*, 2015, **27**, 5995–6001.
- 21 K. R. Deng, J. X. Qin, S. J. Wang, S. Ren, D. M. Han, M. Xiao and Y. Z. Meng, *Small*, 2018, **14**, 1801420.
- 22 C. Z. Zhao, X. Q. Zhang, X. B. Cheng, R. Zhang, R. Xu, P. Y. Chen, H. J. Peng, J. Q. Huang and Q. Zhang, *Proc. Natl. Acad. Sci. U. S. A.*, 2017, **114**, 11069–11074.
- 23 P. E. Trapa, A. B. Reyes, D. R. Sadoway, A. M. Mayes and D. R. Sadoway, *J. Electrochem. Soc.*, 2006, **153**, A1098–A1101.
- 24 Z. L. Hu, S. Zhang, S. M. Dong, Q. Li, G. L. Cui and L. Q. Chen, *Chem. Mater.*, 2018, **30**, 4039–4047.
- 25 Y. Gao, Y. M. Zhao, Y. C. Li, Q. Q. Huang, T. E. Mallouk and D. H. Wang, *J. Am. Chem. Soc.*, 2017, **139**, 15288–15291.
- 26 J. Zhang, C. Ma, Q. Xia, J. Liu, Z. Ding, M. Xu, L. Chen and W. Wei, *J. Membr. Sci.*, 2016, **497**, 259–269.
- 27 X. X. Zeng, Y. X. Yin, N. W. Li, W. C. Du, Y. G. Guo and L. J. Wan, *J. Am. Chem. Soc.*, 2016, **138**, 15825–15828.
- 28 G. M. Zhou, F. Li and H. M. Cheng, *Energy Environ. Sci.*, 2014, **7**, 1307–1338.
- 29 J. J. Zhang, X. Zang, H. J. Wen, T. T. Dong, J. C. Chai, Y. Li, B. B. Chen, J. W. Zhao, S. M. Dong and J. Ma, *J. Mater. Chem. A*, 2017, **5**, 4940–4948.
- 30 J. C. Chai, Z. H. Liu, J. Ma, J. Wang, X. C. Liu, H. S. Liu, J. J. Zhang, G. L. Cui and L. Q. Chen, *Adv. Sci.*, 2017, **4**, 1600377.
- 31 D. C. Lin, P. Y. Yuen, Y. Y. Liu, W. Liu, N. Liu, R. H. Dauskardt and Y. Cui, *Adv. Mater.*, 2018, **30**, 1802661.
- 32 L. Chen, W. X. Li, L. Z. Fan, C. W. Nan and Q. Zhang, *Adv. Funct. Mater.*, 2019, 1901047.
- 33 H. Y. Huo, B. Wu, T. Zhang, X. S. Zheng, L. Ge, T. W. Xu, X. X. Guo and X. L. Sun, *Energy Storage Materials*, 2019, **18**, 59–67.
- 34 X. Zhang, T. Liu, S. F. Zhang, X. Huang, B. Q. Xu, Y. H. Lin, B. Xu, L. L. Li, C. W. Nan and Y. Shen, *J. Am. Chem. Soc.*, 2017, **139**, 13779–13785.
- 35 W. J. Tang, S. Tang, X. Z. Guan, X. Y. Zhang, Q. Xiang and J. Y. Luo, *Adv. Funct. Mater.*, 2019, **29**, 1900648.
- 36 C. Ma, J. F. Zhang, M. Q. Xu, Q. B. Xia, J. T. Liu, S. Zhao, L. B. Chen, A. Q. Pan, D. G. Ivey and W. F. Wei, *J. Power Sources*, 2016, **317**, 103–111.
- 37 J. Shim, D. G. Kim, H. J. Kim, J. H. Lee and J. C. Lee, *ACS Appl. Mater. Interfaces*, 2015, **7**, 7690–7701.
- 38 P. Yuan, C. L. Cai, J. Y. Tang, Y. Q. Qin, M. Y. Jin, Y. B. Fu, Z. H. Li and X. H. Ma, *Adv. Funct. Mater.*, 2016, **26**, 5930–5939.
- 39 M. D. Tikekar, L. A. Archer and D. L. Koch, *Sci. Adv.*, 2016, **2**, e1600320.
- 40 P. Wang, J. C. Chai, Z. H. Zhang, H. R. Zhang, Y. Ma, G. J. Xu, H. P. Du, T. M. Liu, G. C. Li and G. L. Cui, *J. Mater. Chem. A*, 2019, **7**, 5295–5304.